Mössbauer, magnetization and crystal structure studies of the double perovskites $Sr_2FeMo_{1-x}W_xO_6$, x = 0, 0.1, 0.2, 0.3 and 0.4

2002 J. Phys.: Condens. Matter 14 12611

(http://iopscience.iop.org/0953-8984/14/47/332)

INSTITUTE OF PHYSICS PUBLISHING JOURNAL OF PHYSICS: CONDENSED MATTER

J. Phys.: Condens. Matter **14** (2002) 12611–12627 PII: S0953-8984(02)39866-7

Mössbauer, magnetization and crystal structure studies of the double perovskites $Sr_2FeMo_{1-x}W_xO_6$, $x = 0, 0.1, 0.2, 0.3$ and 0.4

A P Douvalis[1], M Venkatesan[1], J M D Coey[1], M Grafoute[2], J-M Greneche[2] and R Suryanarayanan[3]

[1] Physics Department, Trinity College, Dublin 2, Republic of Ireland
[2] Laboratoire de Physique de l'Etat Condensé, UMR 6087 CNRS, Université du Maine, 72085 Le Mans, France
[3] Laboratoire de Physico-Chimie de l'Etat Solide, CNRS, UMR 8648, Bât. 414, Université Paris-Sud, 91405 Orsay, France

E-mail: jcoey@tcd.ie

Received 19 July 2002
Published 15 November 2002
Online at stacks.iop.org/JPhysCM/14/12611

Abstract

The structural, magnetic and electronic properties of the double perovskite series $Sr_2FeMo_{1-x}W_xO_6$, where $x = 0$, 0.1, 0.2, 0.3 and 0.4, are investigated using x-ray diffraction, Mössbauer spectroscopy and magnetization measurements. The crystal structure has been studied at 450 K and at room temperature. There is a structural transition from tetragonal to cubic for $x \leqslant 0.2$. The Curie temperature (T_C) shows a slight increase for $x = 0.1$ and 0.2 ($T_C = 435$ and 432 K, respectively), compared to the value ($T_C = 415$ K) of the $x = 0$ end member. The largest magnetoresistance at 300 K was found for the $x = 0$ and 0.2 compounds. The concentration of antisite defects determined by Mössbauer spectroscopy and x-ray analysis indicate that: (i) cation ordering at the B sites improves with increasing W content and (ii) the antisite defects formed in the B sites of the double perovskite structure do not aggregate to form bigger intragrain clusters with different local chemical compositions. The x dependence of the magnetic moment, which exceeds 4 μ_B per formula unit when $x > 0.3$, is explained in a ferrimagnetic model with, respectively, antiparallel and parallel coupling of antisite iron and molybdenum to their iron or molybdenum cation neighbours. There is a small contribution of 0.2 μ_B/W to the $\downarrow$ sublattice moment. The W-containing materials are not half-metallic.

1. Introduction

Interest in the double perovskite series of formula A_2FeMO_6 (A = Ca, Sr, Ba; M = Mo, W, Re) has revived in recent years [1–5]. This is because some of these compounds are reported to be ferrimagnetic half-metals [1, 2], showing rather good magnetoresistive properties at 300 K [6]

and a Curie temperature higher than those of ferromagnetic mixed-valence manganites [7]. These materials have potential for magnetic sensor applications [8]. The half-metallic property of Sr_2FeMoO_6, which has a T_C about 420 K [1, 9], is reported to depend sensitively on (Fe, Mo) cation disorder at the B sites of the $A_2BB'O_6$ double perovskite structure [10–12]. Different preparation processes can lead to formation of this phase with different amounts of antisite defects [13], but a completely (100%) B site ordered half-metallic Sr_2FeMoO_6 phase remains very difficult to achieve. On the other hand, the double perovskite Sr_2FeWO_6 has been reported to have a highly ordered NaCl-type B site structure of Fe^{2+} and W^{6+} cations [14], but this compound is an antiferromagnetic insulator, with $T_N \approx 40$ K [14, 15]. The introduction of W ions substituting the Mo ions in $Sr_2FeMo_{1-x}W_xO_6$ is reported to improve the B site Fe, Mo/W ordering [14] while the compounds remain metallic over a wide range of W concentrations ($0 < x < 0.7$) [16–18].

In the light of this information, we have prepared a series of $Sr_2FeMo_{1-x}W_xO_6$ double perovskites with low W content ($x = 0$, 0.1, 0.2, 0.3 and 0.4), with a view to investigate the magnetization and B site ordering. We use ^{57}Fe Mössbauer spectrometry to provide information on the intrinsic electronic, magnetic and structural properties of iron ions, which play a central role in the magnetization of these compounds [1, 2].

2. Experimental details

The polycrystalline bulk $Sr_2FeMo_{1-x}W_xO_6$ samples with $x = 0$, 0.1, 0.2, 0.3 and 0.4 were prepared by solid-state reaction. Stoichiometric amounts of high purity oxides and carbonates were calcined at 980 °C, and then reground and refired, with a final firing at 1100 °C in a flowing gas mixture of 1% H_2 in Ar. X-ray diffraction (XRD) diagrams were collected at room temperature (RT: 300 K) and 450 K using Cu Kα radiation in a Siemens D500 diffractometer equipped with a high-temperature set-up. To establish the crystal structure of the samples at 300 and 450 K the XRD diagrams were refined by the Rietveld method, using the GSAS package [19]. ^{57}Fe Mössbauer spectra were collected in transmission geometry from 4.2 to 475 K using an Oxford cryostat and a home-made cryofurnace. The constant acceleration mode spectrometer was equipped with a ^{57}Co(Rh) source maintained at RT. The spectrometer was calibrated using α-Fe, and all isomer shifts are given relative to α-Fe at RT. The spectra were fitted using the least-squares program MOSFIT [20]. For the magnetization measurements a 5 T SQUID (Quantum Design, MPMS XL) magnetometer was used. Magnetoresistance measurements were performed by the four-probe method at RT and 77 K using a 2 T Multimag system (Magnetic Solutions Ltd) equipped with a cryostat for low temperature measurements.

3. Mössbauer spectrometry

Mössbauer spectra were collected at several temperatures between 4.2 and 475 K: representative data are shown in figure 1. At 4.2 K one observes magnetic Zeeman sextets with well-resolved Lorentzian lines, but two magnetic components are needed to describe each spectrum. The fitted parameters are listed in table 1. The main component, with the larger absorption area in each spectrum, exhibits a greater isomer shift (δ) and a smaller hyperfine magnetic field (B_{hf}) than expected for localized $3d^5$ Fe^{3+} ions in octahedral oxygen coordination at 4.2 K [21–23]. On the other hand, the secondary component with the lower absorption area shows δ and B_{hf} values closer to those expected for localized ferric ions, whatever the W content. The same features are observed at 77 K and up to ~150 K. As the temperature is raised above 150 K, the lines of all spectra start to broaden asymmetrically.

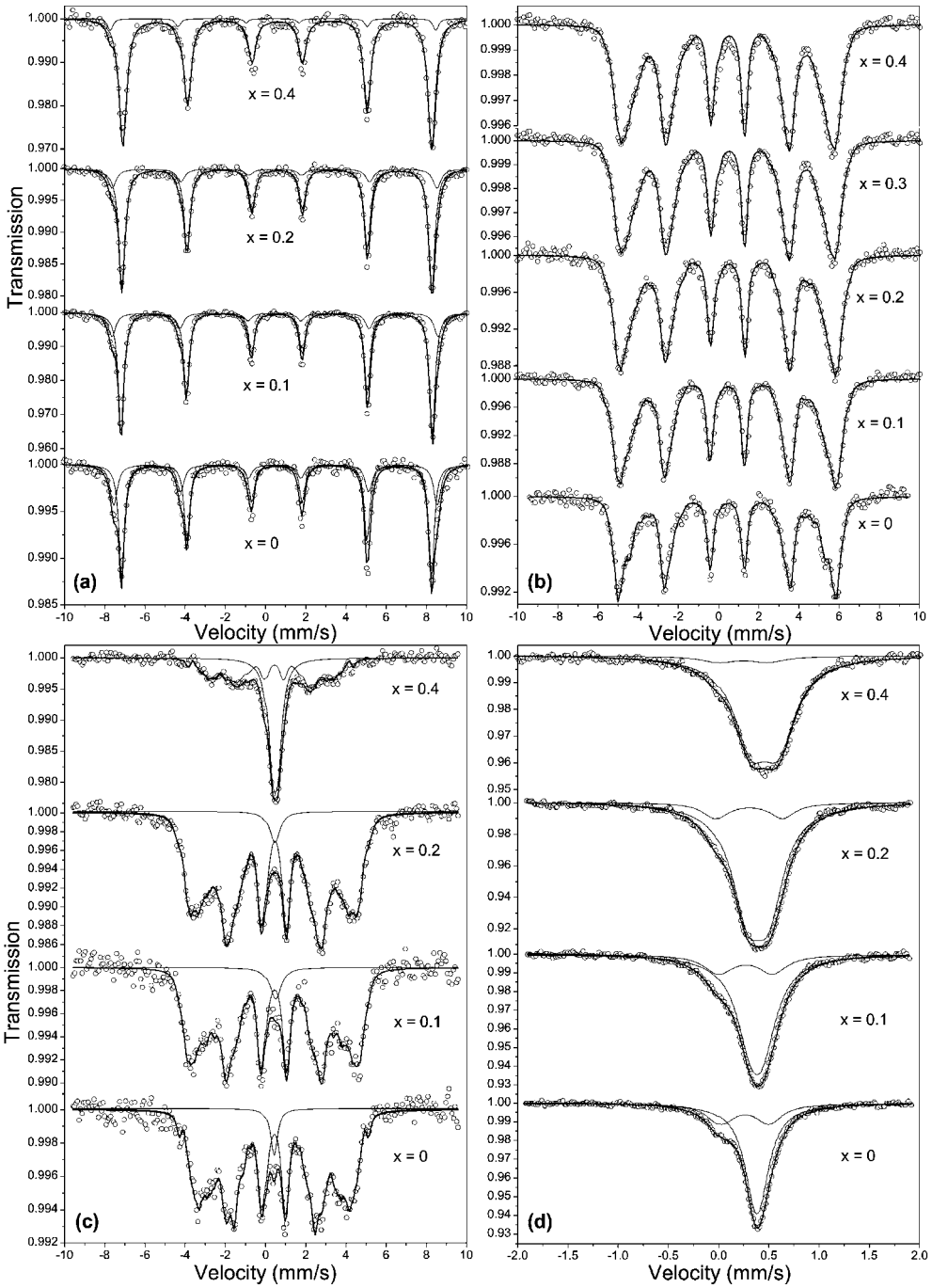

Figure 1. Mössbauer spectra of $Sr_2FeMo_{1-x}W_xO_6$ recorded at several temperatures: (a) 4.2 K, (b) 300 K, (c) 373 K and (d) 475 K. The full curves correspond to the best fits of the experimental data.

To describe both the broadening and the asymmetry of sextet lines we used a distribution of hyperfine fields linearly correlated to a distribution of isomer shifts. The B_{hf} probability

Table 1. Refined values of the Mössbauer parameters of $Sr_2FeMo_{1-x}W_xO_6$ compounds recorded at different temperatures. δ: isomer shift relative to α-Fe at 300 K, $\Delta = e^2qQ[(1+\eta^2/3)^{1/2}]/2$: quadrupole splitting corresponding to the paramagnetic components, $2\varepsilon = e^2qQ(3\cos^2\theta - 1)/4$: quadrupole shift corresponding to the magnetic components, B_{hf}: hyperfine magnetic field, $\Gamma/2$: half linewidth, A: relative absorption area. The antisite concentration (p) deduced from the absorption areas of the secondary components, the corresponding T_C values and the effective valence v for each compound are also listed. Typical errors are ± 0.01 mm s^{-1} for δ, Δ, 2ε, and $\Gamma/2$, ± 0.5 T for B_{hf}, $\pm 3\%$ for A, $\pm 0.5\%$ for p and ± 3 K for T_C. The error on v is $< \pm 0.1$.

x	T (K)	δ (mm s^{-1})	$\langle\delta\rangle$ (mm s^{-1})	Δ or 2ε (mm s^{-1})	B_{hf} (T)	$\langle B_{hf}\rangle$ (T)	$\Gamma/2$ (mm s^{-1})	A (%)	p (%)	T_C (K)	Effective valence v
0	4.2	0.71	0.67	−0.01	47.6	48.3	0.16	68	5.3	415	2.7+
		0.59		0.04	50.0		0.21	32			
	300		0.57	−0.01		30.7		100			
	475	0.48		0.05			0.13	71			
		0.38		0.48			0.15	29			
0.1	4.2	0.71	0.69	−0.01	47.9	48.3	0.16	82	3.0	435	2.7+
		0.60		0.03	50.2		0.22	18			
	300		0.59	−0.01		32.4		100			
	475	0.49		0.13			0.17	81			
		0.38		0.53			0.17	19			
0.2	4.2	0.72	0.71	−0.01	47.7	48.0	0.18	89	1.8	432	2.7+
		0.59		−0.03	50.0		0.23	11			
	300		0.62	0.01		31.7		100			
	475	0.50		0.21			0.18	88			
		0.42		0.65			0.20	12			
0.3	4.2	0.73	0.71	−0.01	47.6	47.8	0.21	92	1.2		2.7+
		0.53		0.01	50.0		0.18	8			
	300		0.60	−0.01		30.0		100			
0.4	4.2	0.75	0.74	−0.01	47.5	47.6	0.22	94	1.0	398	2.7+
		0.52		0.02	50.1		0.15	6			
	300		0.61	−0.01		27.1		100			
	475	0.57		0.27			0.21	93			
		0.36		0.49			0.21	7			

distribution plots resulted from the fits at 300 K are shown in figure 2. The correlation between hyperfine field and isomer shift has been established experimentally in a range of double perovskites [12]. Both are mostly related to the s-electron density at the nucleus. Above 300 K the spectral lines become broader and very complex. An absorption contribution appears at the centre of each spectrum. Although the resolution at these temperatures is poor, this contribution seems to consist of a single paramagnetic line. In order to fit these spectra we include a paramagnetic component. Above T_C, in the pure paramagnetic temperature region, the spectra show resolved spectral lines for all compositions; each spectrum is fitted with two paramagnetic doublets, which are related to the two magnetic sextets observed at low temperatures.

In the perfectly ordered double perovskite crystal structure, the iron ions occupy a single crystallographic site (B), while Mo (or Mo and W) ions occupy the other site (B′), giving rise to a NaCl-type superstructure. However, misplacements where Fe ions change place with Mo (or Mo and W) ions may occur. An example is shown in figure 3. These are known as antisite defects. Following [4, 12] we attribute the main components of the 4.2 K spectra for each compound to iron having an environment of B′site cation neighbours which is composed of six Mo or Mo/W ions, corresponding to the perfectly ordered NaCl-type superstructure.

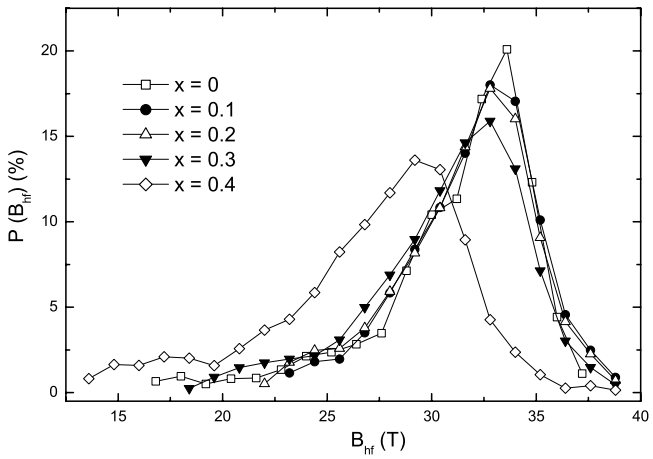

Figure 2. Plots of the hyperfine magnetic field probability distributions deduced from fits of Mössbauer spectra for $Sr_2FeMo_{1-x}W_xO_6$ at 300 K.

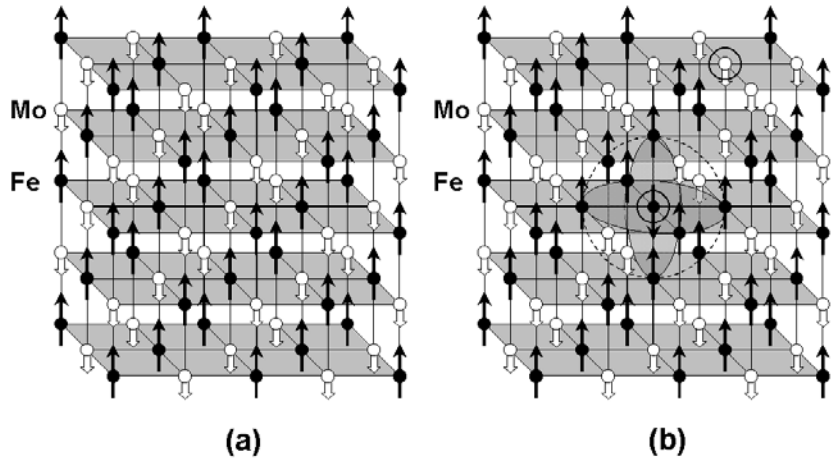

Figure 3. Perfectly ordered NaCl-type superstructure between Fe and Mo ions in Sr_2FeMoO_6 (a), and an example of an antisite defect (b), where the circled iron and molybdenum ions have changed places. The big circles indicate the six first iron neighbours of the antisite defect ion, which contribute a secondary component in the Mössbauer spectra. Sr and O ions are not shown for simplicity.

The secondary component for each compound is attributed to iron ions with a disordered metal–ion environment, which includes one or more Fe, and five or less Mo or Mo/W first metal neighbours, due to antisite defects. In figure 3, there are six of these iron ions on the sphere surrounding the antisite iron. The antisite iron itself has six iron neighbours and gives rise to a weak hyperfine pattern with $B_{hf} \approx 52$ T, which we have not included in the fits, since it is appreciable only for $x = 0$ [24]. The Mo antisite ions do not influence the cation neighbourhood of any of the iron ions.

The higher δ and lower B_{hf} values for the iron ions corresponding to the main components, compared to those of Fe^{3+} ions usually found in oxides [21–23], can be explained by the additional 3d electronic charge density associated with the minority $\downarrow$ electrons, which occupy a narrow conduction band formed by hybridization of Fe(3d)/Mo(4d) and O(2p)

states [1]. This admixture gives the iron ion an effective electronic configuration of $3d^y$, where $5.2 \leqslant y \leqslant 5.4$ [3, 12, 24, 25]. The lower δ and higher B_{hf} values for the iron ions of the secondary components result from the presence of one or more iron ions in their first cation neighbour environment, that decreases the admixture of the hybridized states.

A feature for the Mössbauer spectra is that the relative absorption area of the secondary component is reduced by increasing W content, from 32% for $x = 0$ to 6% for $x = 0.4$. Since each antisite defect creates a modified environment for its six neighbouring iron ions, as shown in figure 3, the concentration of the antisite defects can be deduced at low concentrations as one sixth of the area of the secondary component [4, 12]. Hence we find that the antisite defect concentration p falls from 5.3% for the $x = 0$ compound to 1.0% for the $x = 0.4$ compound (see table 1). There is a continuous enhancement of the Fe, Mo/W cation NaCl-type ordering in the B sites as the W content increases. This confirms the results of previous x-ray and magnetization studies [14, 16, 17].

The distinctive characteristics of the low temperature spectra, which are indicative of the two main iron environments, are lost as the temperature is raised to RT. This broadening of the spectral lines is attributed to the distribution of the different first and more distant metal ion neighbour environments (Mo, Fe, W and all their combinations) which introduces a distribution of exchange coupling, which leads to increased line broadening as the temperature approaches T_C [26]. Above RT a paramagnetic component starts to appear in the Mössbauer spectra of all compounds studied. The temperature above which we had to add the contribution of the paramagnetic component seems to depend on the W content of the compound studied. Thus for the $x = 0.4$ compound this temperature is around 333 K, while for the lower W-doped compounds it is in the region of 373 ± 5 K. The Mössbauer parameters for these paramagnetic components are close to those of the main paramagnetic components used to fit the relative spectra above T_C.

As the temperature is raised further the paramagnetic contribution increases at the expense of the magnetic part of the spectrum. The evolution with temperature of the paramagnetic fraction is shown in figure 4. T_C has been defined as the temperature where we extrapolate to 100% of paramagnetic contribution. These temperatures are included in table 1: the highest T_C of 435 K for $x = 0.1$ is 20 K higher than that of pure Sr_2FeMoO_6. All T_C values were confirmed by thermogravimetric measurements.

Above T_C we observe asymmetric paramagnetic spectra. The asymmetry is reduced as the W content increases. Two paramagnetic components were used to fit the spectra in this region, corresponding to the two different cation environments, as in the case of the 4.2 K spectra. The fitted parameters show that the main component exhibits lower quadrupole splitting (Δ) and higher δ values than the secondary component, whatever the W content. The absorption area of the secondary component is again reduced with increasing W content, and the proportions are consistent with the low-temperature results. However, a new feature is the increasing value of Δ of the main component with increasing W content. The quadrupole splitting of the $x = 0$ compound at 475 K is very close to zero, suggesting accordingly a nearly perfectly cubic arrangement of the oxygen ions in the FeO_6 octahedra, whereas the increased Δ values for the higher W-doped ($x = 0.2$ and 0.4) compounds suggest a reduction in crystal symmetry. This was confirmed by x-ray analysis.

4. Crystal structure studies

The refined x-ray diffractograms of $Sr_2FeMo_{1-x}W_xO_6$ for $x = 0$, 0.1 and 0.4 collected at temperatures of 300 and 450 K are shown in figure 5, and the results of the refinement for all samples are displayed in table 2. The RT structure was refined in the tetragonal $I4/m$ space group, which was used successfully by Chmaissem *et al* [27] for the refinement of the

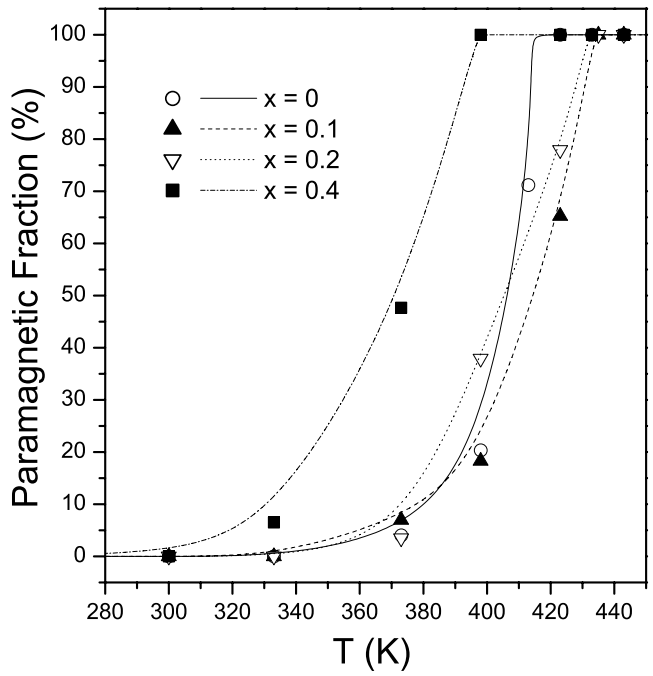

Figure 4. Temperature variation of the total paramagnetic fraction of the fitted Mössbauer spectra of $Sr_2FeMo_{1-x}W_xO_6$ for $x = 0$, 0.1, 0.2 and 0.4. The relative curves are a guide to the eye for the variation corresponding to each composition.

neutron diffraction pattern of Sr_2FeMoO_6. There is an evolution of the crystal structure for all compounds between 300 and 450 K, which is evident in figure 6, where a magnification of the high angle region ($100° < 2\theta < 115°$) of the diffractograms is shown. The reduction of the number of high angle reflections, corresponding to crystal planes with *hkl* indices (008), (440), (028), (336), (352) and (060) of the 450 K patterns for all compounds, shows that the structure is transformed to a more symmetric one. We have refined the 450 K diffractograms using both the tetragonal $I4/m$ and the cubic *Fm3m* space groups (see table 2). It is known that a tetragonal to cubic crystal structure transition occurs at 400 K in the end member [27, 28], and it is evident from our data that a similar transition also occurs for the W-doped compounds. However, attempts to refine the 450 K diffractograms using *Fm3m* gave an acceptable set of values for the refinement reliability factors (R_p, R_{wp}, R_{F^2}), only for $x = 0$, 0.1 and 0.2. This means that the tetragonal to cubic transformation is complete at 450 K only for low W doping. This is even more evident from the number of peaks in the higher 2θ range ($100° < 2\theta < 115°$) of the 450 K patterns for the $x = 0.3$ and 0.4 samples shown in figure 7, which cannot be explained in the cubic space group. In order to display the nature of this structural evolution for each compound, we have plotted in figure 8(a) the quantity $(1 - a\sqrt{2}/c)$ versus x, for both the low and high temperature structures, when all refinements were done using $I4/m$. Near-zero values corresponding to the 450 K cubic structures are found for $x = 0$ and 0.1. The values for the other samples diverge more from zero and indicate an evolution of the tetragonal RT structure to a more 'symmetric' tetragonal structure for the higher W-doped compounds rather than a transition to the cubic structure, at least at 450 K. In figure 8(b) the a and c axis values are plotted versus x both for RT and 450 K structures. These results are consistent with other data [14, 16] for these materials.

Table 2. Values of the unit-cell parameters resulting from the refinement of the XRD patterns of the $Sr_2FeMo_{1-x}W_xO_6$ compounds using the tetragonal $I4/m$ and the cubic $Fm3m$ space groups as described in the text. The $(1 - a\sqrt{2}/c)$ values, the relative reliability factors and the occupancies of the B and B′sites for each refinement are also listed. The numbers in parentheses are standard deviations referred to the last digit for each value.

									Occupancy B site			Occupancy B′site		
x	T (K)	Space group	a (Å)	c (Å)	$1 - a\sqrt{2}/c$	R_p	R_{wp}	R_{F^2}	Fe	Mo	W	Fe	Mo	W
	300	$I4/m$	5.579 71(3)	7.913 95(7)	0.002 91	6.52	9.08	3.94	0.940(2)	0.060(2)	—	0.060(2)	0.940(2)	—
0	450	$I4/m$	5.594 91(6)	7.909 6(2)	−0.000 35	7.06	10.23	7.7	0.946(2)	0.054(2)	—	0.054(2)	0.946(2)	—
	450	$Fm3m$	7.911 40(7)			7.34	10.46	4.8	0.942(3)	0.058(3)	—	0.058(3)	0.942(3)	—
	300	$I4/m$	5.579 91(7)	7.918 3(1)	0.003 43	6.36	9.02	4.3	0.955(3)	0.041(2)	0.005(1)	0.045(3)	0.859(2)	0.095(1)
0.1	450	$I4/m$	5.597 2(1)	7.913 8(4)	−0.000 23	7.01	9.78	3.86	0.954(2)	0.041(2)	0.005(2)	0.046(2)	0.859(2)	0095(1)
	450	$Fm3m$	7.915 11(7)			7.39	10.15	5.02	0.963(3)	0.033(2)	0.004(1)	0.037(3)	0.867(2)	0.096(1)
	300	$I4/m$	5.580 0(1)	7.919 8(2)	0.003 60	4.80	3.70	7.73	0.980(3)	0.016(2)	0.004(1)	0.020(3)	0.784(2)	0.196(1)
0.2	450	$I4/m$	5.597 7(1)	7.921 19(3)	0.000 62	6.58	7.95	7.46	0.998(3)	0.001(2)	0.001(2)	0.002(2)	0.788(2)	0.200(2)
	450	$Fm3m$	7.918 44(9)			6.55	8.04	4.4	0.987(3)	0.011(2)	0.003(1)	0.013(3)	0.789(2)	0.197(1)
	300	$I4/m$	5.583 31(7)	7.928 9(1)	0.004 16	5.52	6.96	4.52	0.998(2)	0.001(2)	0.001(2)	0.002(2)	0.698(2)	0.300(2)
0.3	450	$I4/m$	5.599 20(8)	7.930 0(2)	0.001 46	6.77	8.51	5.39	0.990(2)	0.007(2)	0.003(1)	0.010(2)	0.693(2)	0.297(2)
	450	$Fm3m$	7.921 7(1)			7.67	9.77	5.85	0.989(3)	0.008(2)	0.003(1)	0.011(2)	0.692(2)	0.297(2)
	300	$I4/m$	5.583 90(8)	7.934 0(1)	0.004 69	6.48	8.07	4.35	0.986(2)	0.008(1)	0.006(1)	0.014(2)	0.592(2)	0.394(2)
0.4	450	$I4/m$	5.600 81(9)	7.937 9(2)	0.002 16	6.93	8.74	4.53	0.993(3)	0.004(3)	0.003(3)	0.007(3)	0.596(2)	0.397(2)
	450	$Fm3m$	7.926 2(2)			8.96	11.62	4.61	0.983(2)	0.010(2)	0.007(1)	0.017(2)	0.590(2)	0.393(1)

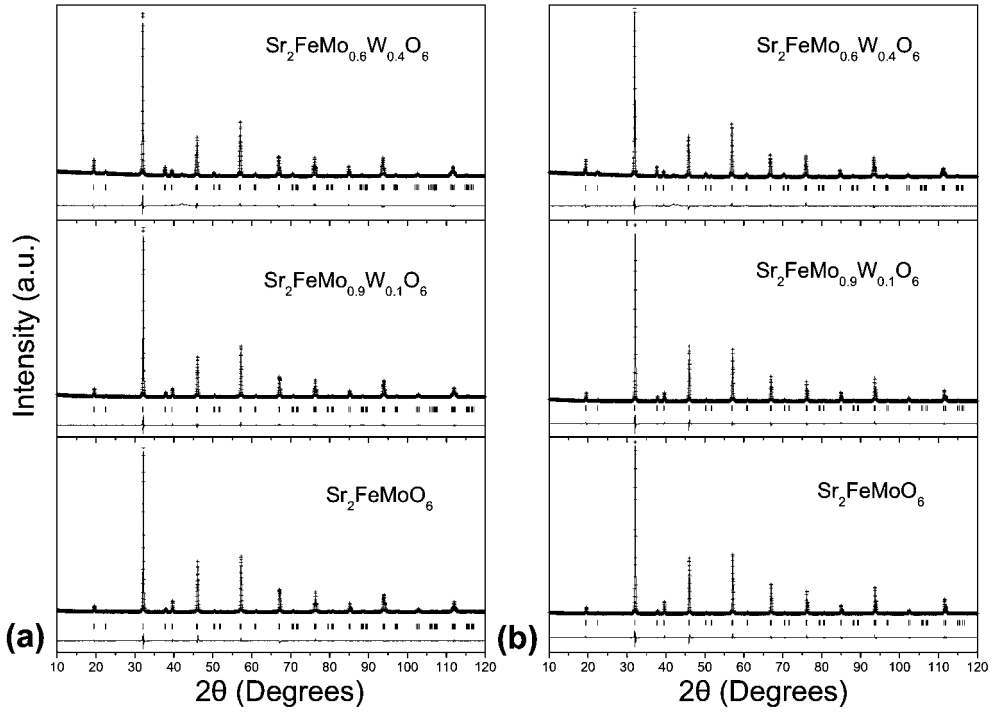

Figure 5. XRD refined patterns of selected $Sr_2FeMo_{1-x}W_xO_6$ compounds at 300 K (a) and 450 K (b). The experimental points appear as crosses and the theoretical model corresponds to the full curve. The difference between the experimental data and the fits is displayed, and the theoretical reflection positions at the relative 2θ angles are denoted by vertical bars.

The antisite concentration was independently determined by analysis of the diffractograms using the Rietveld method. Initial values of p were taken from the Mössbauer data. At the end of the Rietveld refinement the refined site occupancies (see table 2) turned out to be very close to the starting ones in all cases, which confirms the interpretation of the Mössbauer spectra.

5. Magnetization studies

The isothermal M versus H curves taken at 5 K for each compound are shown in figure 9. The saturation moments per formula unit (M_S) increase with increasing W content as shown in figure 10. For the $x = 0, 0.1$ and 0.2 compounds the values are below 4.0 μ_B/fu, while for the $x = 0.3$ and 0.4 compounds they exceed 4.0 μ_B/fu. We observed no coercivity or remanence for any of the compounds, even at 5 K.

The antisite defects are expected to have a major influence on the saturation moment [3, 4, 12, 14, 17, 29]. We consider several different models in order to account for the trend in figure 10. In every case we use the concentrations of antisite defects (p) deduced from the Mössbauer data and x-ray refinements to calculate the M_S values expected for each composition. The experimental error on M_S is ± 0.02 μ_B/fu.

The points at issue are:

(i) the charge state of the iron,
(ii) whether or not the molybdenum and tungsten possess a moment, and
(iii) how that moment is oriented on the B site antisite defects.

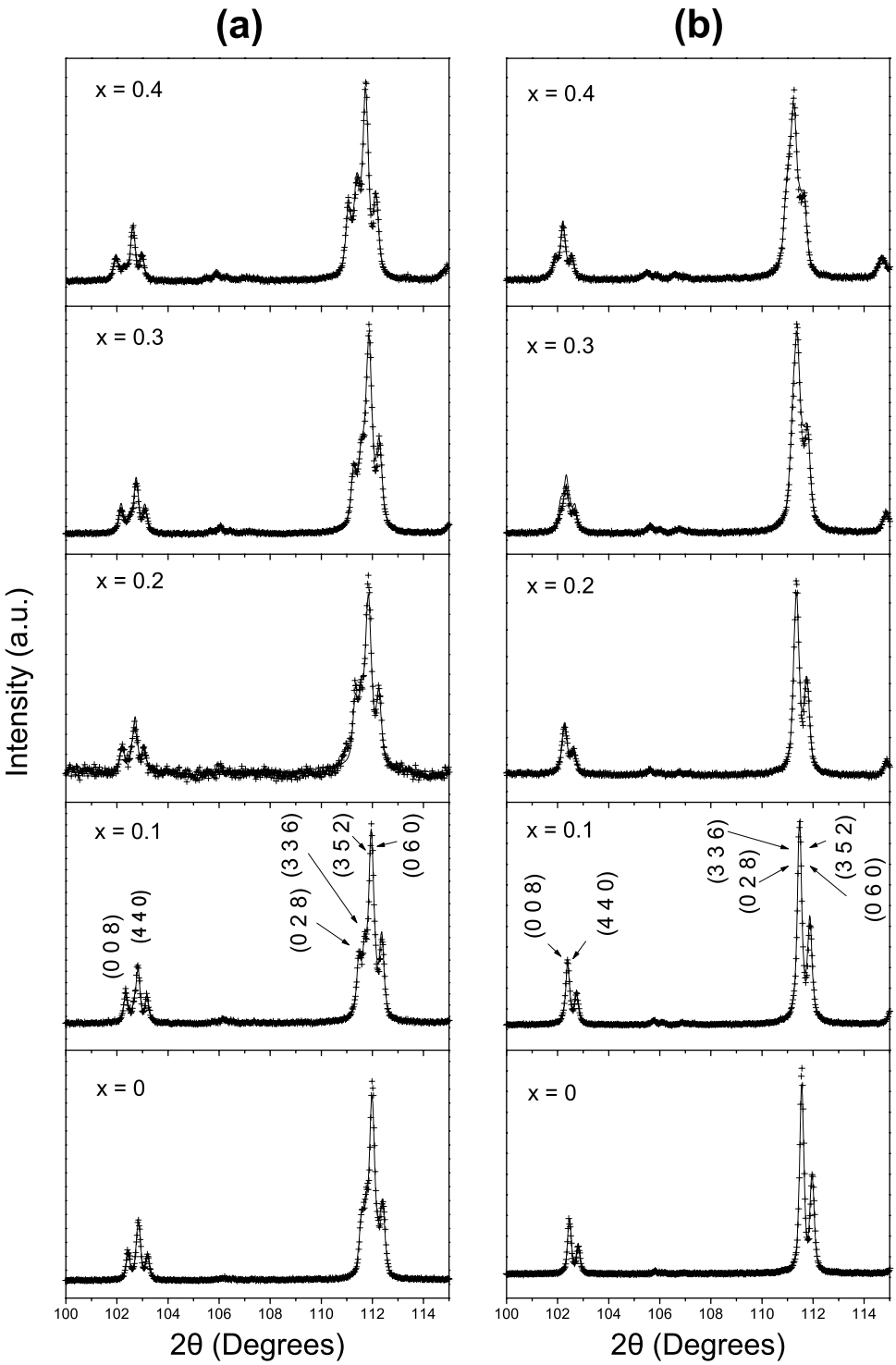

Figure 6. Magnification of the $100° < 2\theta < 115°$ part of the refined XRD patterns of the $Sr_2FeMo_{1-x}W_xO_6$ samples using the tetragonal space group $I4/m$ at 300 K (a) and 450 K (b). The differences in the number of diffraction peaks for the two temperature patterns are evident.

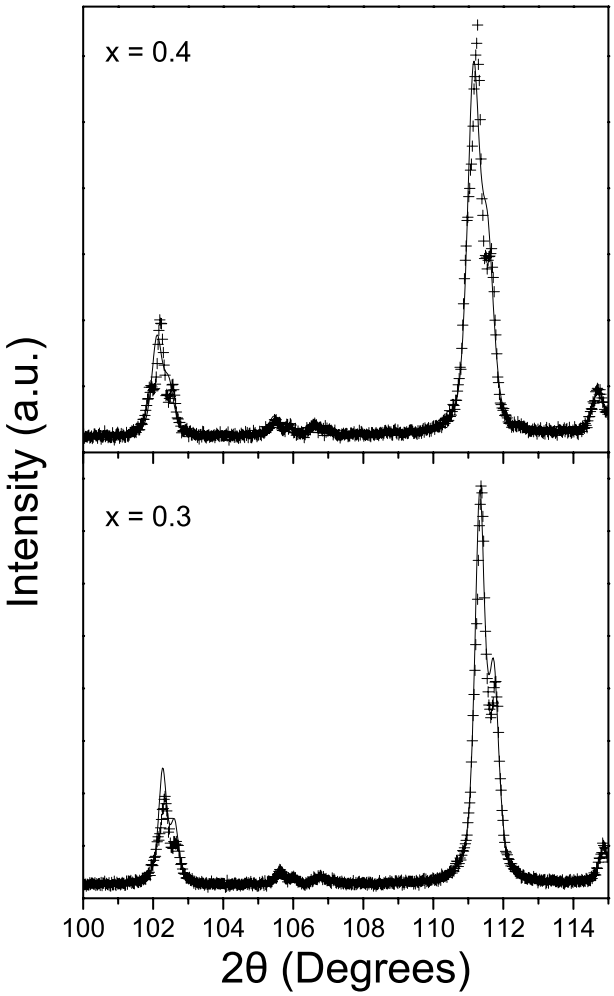

Figure 7. The $100° < 2\theta < 115°$ part of the patterns of the $Sr_2FeMo_{1-x}W_xO_6$ samples for $x = 0.3$ and 0.4 at 450 K, refined using the cubic *Fm3m* space group. The fit to the experimental data is worse than that found using the tetragonal $I4/m$ space group as shown in figure 6.

We suppose that the B′antisite defects (iron with six iron neighbours) is bound to couple antiferromagnetically to its six iron neighbours on account of the 180° superexchange bonds, according to the Goodenough–Kanamori rules [30].

A first model puts no moment on the B′ ions, except when they are occupied by antisite iron. The antisite iron is supposed to be Fe^{3+}, with a full spin moment of 5 μ_B. The normal B site iron has valence v and a spin moment of $(2 + v)$ μ_B. The valence v, deduced from the isomer shift using the formula $v = 3 - \{(\delta - \delta_{Fe^{3+}})/(\delta_{Fe^{2+}} - \delta_{Fe^{3+}})\}$, where $\delta_{Fe^{3+}} = 0.52$ mm s^{-1} and $\delta_{Fe^{2+}} = 1.20$ mm s^{-1} [24], is +2.7 (see table 1). The calculated moment is then

$$M_S = (2 + v)(1 - p) - 5p\ \mu_B/\text{fu}. \tag{1}$$

This model seriously overestimates M_S, by about 0.6 μ_B/fu (figure 10).

The second model assumes that the B′site molybdenum and tungsten both have a moment of $(2 - v)$ μ_B and the antisite molybdenum (or tungsten) contributes -1 μ_B. It is coupled

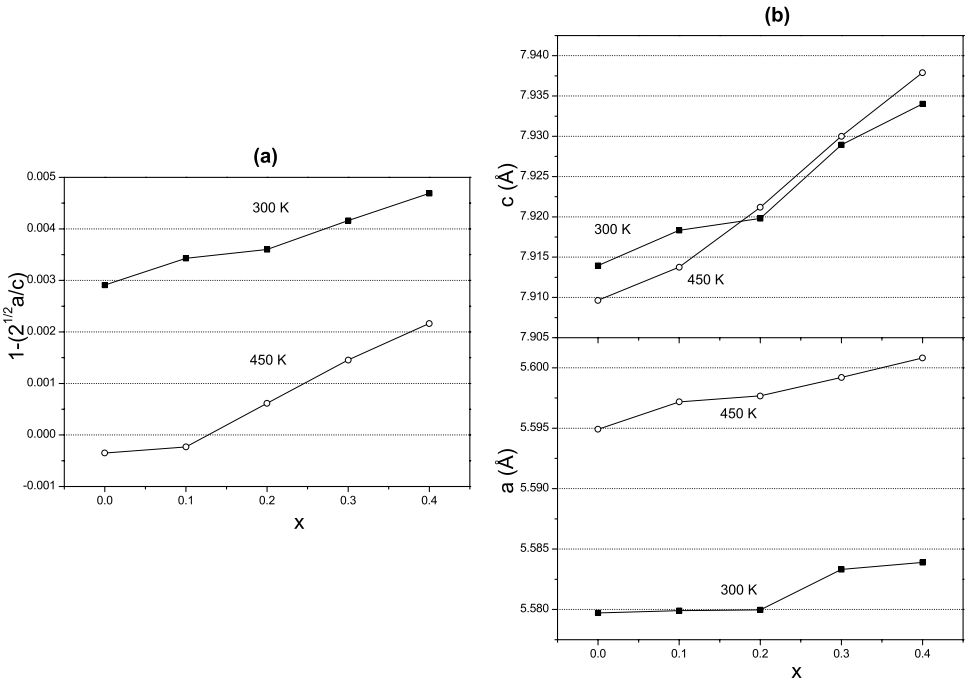

Figure 8. Variation of the distortion parameter $(1 - a\sqrt{2}/c)$ (a) and the tetragonal a and c axes (b) with W content x at 300 K and 450 K.

parallel to its molybdenum neighbours [30, 31]. There is therefore spin conservation between iron and molybdenum in a fully spin polarized 3d t_{2g} (Fe)/t_{2g} (Mo, W) minority-spin band. The moment in μ_B per formula unit is

$$M_S = (4 - 10p). \tag{2}$$

This is now independent of the iron valence, and the same result is obtained if we allow for different values of the iron sites with (6 Mo) or (5 Mo, 1 Fe) neighbours, because corresponding charges appear on the molybdenum/tungsten sites with (6 Fe) neighbours and (5 Fe, 1 Mo) neighbours. This half-metallic model reproduces correctly the end member moment but underestimates those of the W-doped compounds. The same result is obtained assuming that the tungsten forms non-magnetic W^{6+} ($5d^0$) ions, and that an equivalent amount of Fe^{3+} is transformed to Fe^{2+} to ensure charge neutrality. Note that the magnetization can, in no case, exceed 4.0 μ_B/fu with these models, while in practice the magnetization reaches 4.12 μ_B/fu when $x = 0.4$.

If the antisite Mo were coupled antiparallel to its six Mo neighbours, the moment in μ_B per formula unit would be greater:

$$M_S = (4 - 8p) \tag{3}$$

but it does not fit the data on the end member (figure 10).

A third model assigns no moment to the W ions. We adjust 5d electrons on the tungsten, but suppose the 5d band has no spin polarization. In that case the expression for the moment in μ_B per formula unit is

$$M_S = 4 - 10p - x(2 - v + vp - 3p). \tag{4}$$

Comparison with the data in figure 10 shows that the third model with an antisite moment of -1 μ_B comes close to reproducing the experimental results. By admitting a slight spin

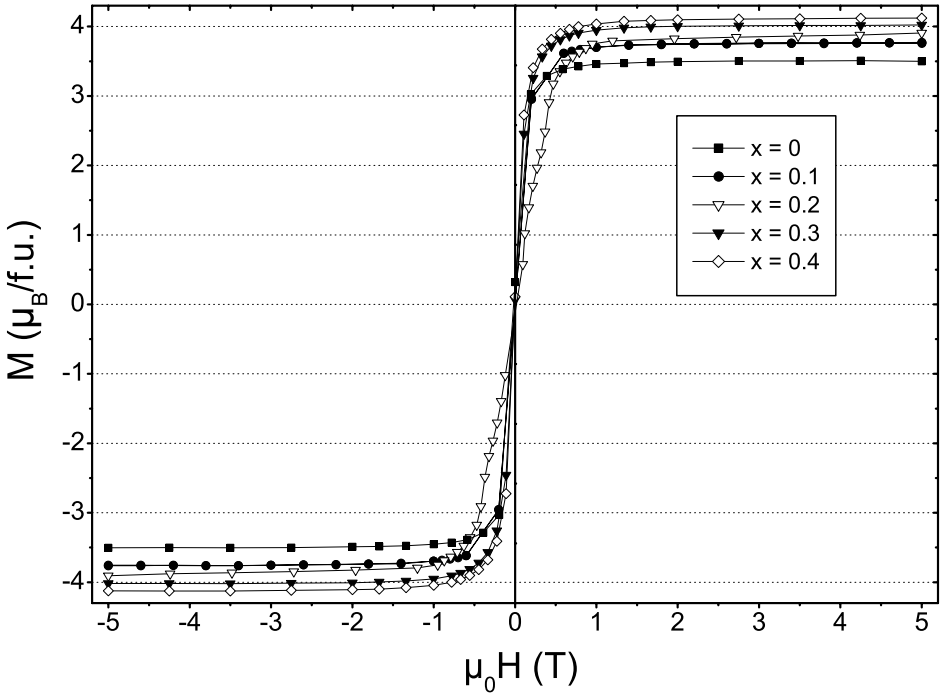

Figure 9. Isothermal magnetization curves of the $Sr_2FeMo_{1-x}W_xO_6$ samples at 5 K.

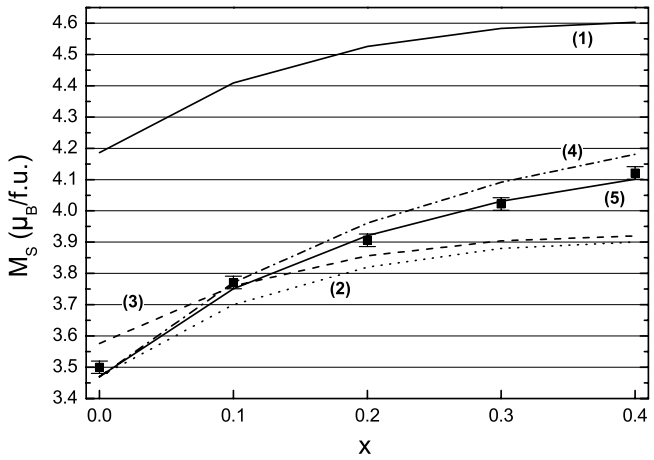

Figure 10. Variation with x of M_S (square points), the saturated moment per formula unit at 5 K and the corresponding predicted M_S values (lines) calculated using the measured concentrations of antisite defects based on the models of equations (1)–(5), as discussed in the text. The best fit (5) is obtained with a minority spin contribution of 1.0 μ_B/Mo and 0.2 μ_B/W.

polarization of the tungsten ($\sim$0.2 μ_B) the expression for the moment in μ_B per formula unit becomes

$$M_S = 4 - 10p - x(2 - v + vp - 3p + 0.2) \tag{5}$$

and the model can be brought into agreement with the experimental data across the complete range of x.

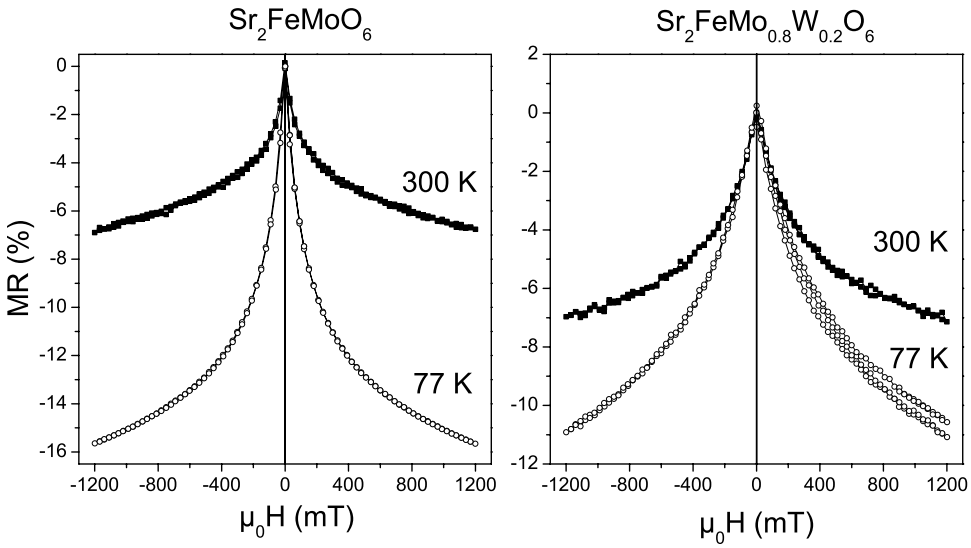

Figure 11. Magnetoresistance of sintered Sr_2FeMoO_6 and $Sr_2FeMo_{0.8}W_{0.2}O_6$ samples at 300 K and 77 K.

Magnetoresistance measurements were made at 300 and 77 K. The relative MR $= ((\rho(0) - \rho(H))/\rho(0))$ versus H curves are shown in figure 11. We have found appreciable MR in an applied field of 1200 mT for the $x = 0$ (7% at 300 and 16% at 77 K) and $x = 0.2$ (7% at 300 and 11% at 77 K) samples. For the $x = 0.1$ sample the effect is smaller and the other compounds ($x = 0.3$ and 0.4) show no appreciable effect. As the magnetoresistive phenomena in these compounds have basically extrinsic character [1, 2, 5] and depend strongly on the nature and composition of the grain boundaries, as well on the nature of the contacts between grains, we can attribute the variability of the magnetoresistance to these factors [17].

6. Discussion

The evolution of the tetragonal crystal structure with temperature from 300 to 450 K has been established for all the $Sr_2FeMo_{1-x}W_xO_6$ double perovskites. For low doping, $x = 0$, 0.1 and 0.2, there is a structural transition from tetragonal at RT to cubic at 450 K, but for $x = 0.3$ and 0.4 compounds the crystal structure remains tetragonal at and above 450 K, as indicated both by the refinement of their x-ray patterns and also by the quadrupole splittings observed above T_C.

There is a clear improvement of the B site ordering of the Fe and Mo/W ions as the W composition is increased, evident by the decrease of the relative absorption area of the secondary component in the Mössbauer spectra. The isomer shifts for the main component used to fit the 4.2 K spectra are greater than those expected for high spin ($S = 5/2$) Fe^{3+} $3d^5$ ions in an octahedral oxygen environment [21–23], but they are not large enough to correspond to a $Fe^{2.5+}$ mixed valence state, as was found for Ba_2FeMoO_6 [12, 24]. The iron valence is 2.7+ and there is a little variation with W content up to $x = 0.4$. The iron charge state in Sr_2FeMoO_6 arises from the half-metallic structure where there is a full 3d ↑ band and a ↓ minority-spin band which is formed by hybridization of the Fe 3d ↓ and Mo 4d ↓ with the O 2p orbitals [1, 5, 10, 32]. For low to intermediate W doping values this structure is modified as shown in figure 12, because the W, unlike the Mo, contributes electrons to both ↑

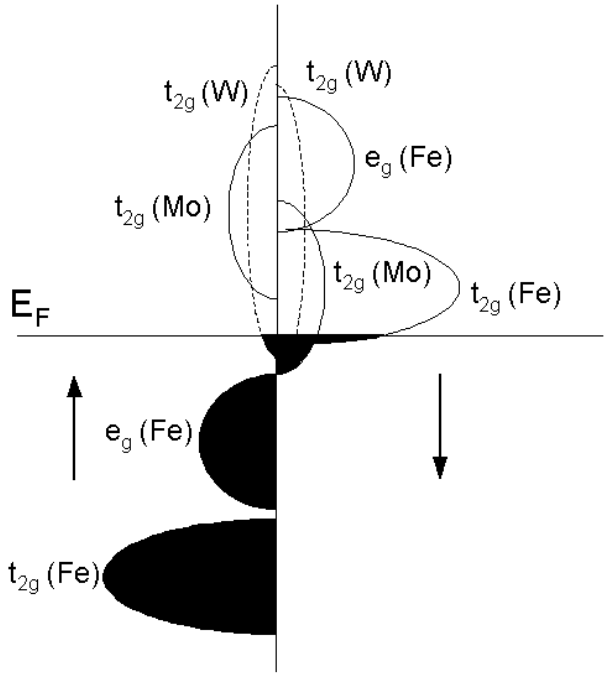

Figure 12. Schematic electronic structure of W-doped Sr_2FeMoO_6. The tungsten ↑ and ↓ density of states are indicated by the broken lines and the Fermi level (E_F) by the horizontal straight line.

and ↓ bands. In this case there is no spin gap and the material is no longer a half-metal. The compounds remain metallic in the range of doping we have investigated, but at high W doping the materials become semiconductors or insulators [14, 17, 18] with the iron in ferrous state. However, there is only a slight increase in the isomer shift $d\delta/dx = 0.1$ mm s^{-1} at 4.2 K in the range $0 \leqslant x \leqslant 0.4$ reflecting a nearly constant iron ion configuration. The measured electronic configuration is an average over the time window associated with the hyperfine interactions, which in the case of ^{57}Fe is of the order of $t_m \sim 10^{-8}$ s [21–23]. The minority ↓ electrons are itinerant, in a band of width $W \approx 1$ eV, which corresponds to a fluctuation time $\hbar/W \ll t_m$. The iron sites with one Fe neighbour lie higher in energy than those with none, and the ↓ electrons spend less time on these sites, leading to the lower isomer shifts.

Another point that follows from our data is that the antisite defects do not aggregate to form clusters of $SrMoO_3$ or $SrFeO_3$. If this was the case, we would observe a hyperfine pattern with distinctive hyperfine parameters $\delta = 0.15$ mm s^{-1}, $2\varepsilon \approx 0$ mm s^{-1}, $B_{hf} = 33.1$ T at 4.2 K [33].

The temperature interval where magnetic and paramagnetic contributions coexist in the spectra, although different for different x values, is in any case quite large. As we found no evidence of secondary phases in our samples, the mixed spectra reflect intrinsic inhomogeneity of the samples themselves. We believe the inhomogeneity is associated with antisite defects and with the W doping, which create a broad distribution of magnetic interactions at the iron sites. This is most evident in $Sr_2FeMo_{0.6}W_{0.4}O_6$, which has the lower T_C. However, aggregation of Sr_2FeWO_6 [14] or $SrFeO_3$ [34] must be ruled out for our samples, because this would have given a characteristic contribution of Fe^{2+} or Fe^{4+}, which is not observed. The formation of more large intragrain homogeneous regions of $Sr_2FeMo_{1-x}W_xO_6$ with x large enough to give

antiferromagnetic character to these parts was also proposed by Linden *et al* [35], but it is also unlikely in our samples, because it would again give characteristic Fe^{2+} subspectra, which are not observed. Nor are $SrFeO_{2.5}$ intragrain clusters likely, because they would have given contributions of Fe^{3+} subspectra quite different to those observed due to the presence of both tetrahedral and octahedral ferric oxygen coordinated sites [33].

Our analysis of the spectra suggests that the antisite defects are present throughout the structure of each grain, but they are rather isolated from each other. They do not cluster to form distinct $SrFeO_3$ or Sr_2FeWO_6 regions with a chemical composition different from the average one.

The increase of T_C for the $x = 0.1$ and 0.2 compounds may be related to the improvement in the B site cation order. As the W concentration is relatively low for these compounds, the W ions do not dilute the Fe–Mo system so much as to cause breakdown of the magnetic interactions, but by the observed improvement of cationic ordering they suppress some of the B′site iron which introduces with it antiferromagnetic coupling.

7. Conclusions

We find that substitution of tungsten in Sr_2FeMoO_6 produces a small increase of the Curie temperature and potentially useful magnetoresistance, despite the loss of half-metallic character on W doping. The tungsten substitution improves the cation ordering at the B and B′ sites. The magnetization is explained by a ferrimagnetic model, which takes account of the antisite defects, and associates a small $\downarrow$ moment contribution of $0.2\ \mu_B$ with the tungsten ions and $1\ \mu_B$ with the Mo ions, although these moments are distributed in a band composed of Fe (t_{2g}), Mo (t_{2g}) and W (t_{2g}) $\downarrow$ orbitals.

Acknowledgments

This work was partly supported by the AMORE project of the EU Growth program, and by the France–Ireland scientific exchange scheme.

References

[1] Kobayashi K-I, Kimura T, Sawada H, Terakura K and Tokura Y 1998 *Nature* **395** 677
[2] Kobayashi K-I, Kimura T, Tomioka Y, Sawada H and Terakura T 1999 *Phys. Rev.* B **59** 11159
[3] Borges R P, Thomas R M, Cullinan C, Coey J M D, Suryanarayanan R, Ben-Dor L, Pinsard-Gaudart L and Revcolevschi A 1999 *J. Phys.: Condens. Matter* **11** L445
[4] Pinsard-Gaudart L, Suryanarayanan R, Revcolevschi A, Rodriguez-Carvajal J, Greneche J-M, Smith P A I, Thomas R M, Borges R P and Coey J M D 2000 *J. Appl. Phys.* **87** 7118
[5] Sarma D D 2001 *Curr. Opin. Solid State Mater. Sci.* **5** 261
Maignan A, Martin C, Hervieu H and Raveau B 2000 *J. Magn. Magn. Mater.* **211** 173
Kang J S, Han H, Lee B W, Olson C G, Han S W, Kim K H, Jeong J I, Park J H and Min B I 2001 *Phys. Rev.* B **64** 024429
Gopalakrishnan J, Chattopadhyay A, Ogale S B, Venkatesan T, Greene R L, Millis A J, Ramesha K, Hannoyer B and Marest G 2000 *Phys. Rev.* B **62** 9538
[6] Venkatesan M, Varadaraju U V, Douvalis A P, Fitzgerald C B, Rhen F M F and Coey J M D 2002 *J. Mater. Chem.* **12** 2184
[7] Coey J M D, Viret M and von Molnar S 1999 *Adv. Phys.* **48** 167
[8] Coey J M D 2001 Materials for spin electronics *Spin Electronics* ed M Ziese and M J Thornton (Berlin: Springer) p 277
[9] Nakagawa T 1968 *J. Phys. Soc. Japan* **24** 806
[10] Saha-Dasgupta T and Sarma D D 2001 *Phys. Rev.* B **64** 064408

[11] Sarma D D, Sampathkumaran E V, Ray S, Nagarajan R, Majumdar S, Kumar A, Nalini G and Guru Row T N 2000 *Solid State Commun.* **114** 465
[12] Greneche J-M, Venkatesan M, Suryanarayanan R and Coey J M D 2001 *Phys. Rev.* B **63** 174403
[13] Balcells L I, Navarro J, Bibes M, Roig A, Martinez B and Fontcuberta J 2001 *Appl. Phys. Lett.* **78** 781
[14] Kobayashi K-I, Okuda T, Tomioka Y, Kimura T and Tokura Y 2000 *J. Magn. Magn. Mater.* **218** 17
[15] Kawanaka H, Hase I, Toyama S and Nishihara Y 2000 *Physica* B **281–282** 518
[16] Dass R I and Goodenough J B 2001 *Phys. Rev.* B **63** 064417
[17] Ray S, Kumar A, Majumdar S, Sampathkumaran E V and Sarma D D 2001 *J. Phys.: Condens. Matter* **13** 607
[18] Nakagawa T, Yoshikawa K and Nomura S 1969 *J. Phys. Soc. Japan* **27** 880
[19] Larson A C and Von Dreele R B 2001 *General Structure Analysis System (Los Alamos National Laboratory, University of California)* (ftp://ftp.lanl.gov/public/gsas/)
[20] Teillet J and Varret F MOSFIT program, University du Maine (unpublished)
[21] Greenwood N N and Gibb T C 1971 *Mössbauer Spectroscopy* (London: Chapman and Hall)
[22] Gütlich P, Link R and Trautwein A 1978 *Mössbauer Spectroscopy and Transition Metal Chemistry* (Berlin: Springer)
[23] Dickson D P E and Berry F (ed) 1986 *Mössbauer Spectroscopy* (Cambridge: Cambridge University Press)
[24] Douvalis A P, Venkatesan M and Coey J M D 2002 *Hyperfine Interact.* at press
[25] Venkatesan M, Grafoute M, Douvalis A P, Greneche J-M, Suryanarayanan R and Coey J M D 2002 *J. Magn. Magn. Mater.* **242–245** 744
[26] Coey J M D 1972 *Phys. Rev.* B **6** 3240
[27] Chmaissem O, Kurk R, Dabrowski B, Brown D E, Xiong X, Kolesnik S, Jorgensen J D and Kimball C W 2000 *Phys. Rev.* B **62** 14197
[28] Ritter C, Ibarra M R, Morellon L, Blasco J, Garcia J and De Teresa J M 2000 *J. Phys.: Condens. Matter* **12** 8295
[29] Ogale A S, Ogale S B, Ramesh R and Venkatesan T 1999 *Appl. Phys. Lett.* **75** 537
[30] Goodenough J B 1963 *Magnetism and the Chemical Bond* (New York: Interscience)
[31] Navarro J, Balcells L I, Bibes M, Roig A, Martinez B and Fontcuberta J 2001 *J. Phys.: Condens. Matter* **13** 8481
[32] Fang Z, Terakura K and Kanamori J 2001 *Phys. Rev.* B **63** 180407(R)
[33] Gallagher P K, MacChesney J B and Buchanan D N E 1964 *J. Chem. Phys.* **41** 2429
[34] Garcia-Hernandez M, Martinez J L, Martinez-Lope M J, Casais M T and Alonso J A 2001 *Phys. Rev. Lett.* **86** 2443
[35] Linden J, Yamamoto T, Nakamura J, Karppinen M and Yamauchi H 2001 *Appl. Phys. Lett.* **78** 2736